

pubs.acs.org/acscatalysis Research Article

# Selective Reduction of Carboxylic Acids to Aldehydes with Promoted MoO<sub>3</sub> Catalysts

Laura A. Gomez, Reda Bababrik, Mallikharjuna R. Komarneni, Justin Marlowe, Taha Salavati-fard, Andrew D. D'Amico, Bin Wang, Phillip Christopher, and Steven P. Crossley\*



Cite This: ACS Catal. 2022, 12, 6313-6324



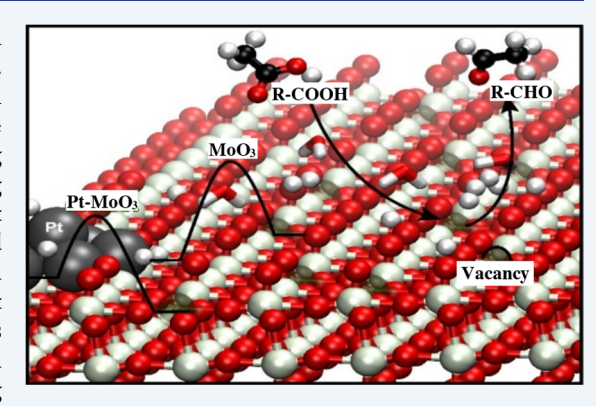
**ACCESS** 

Metrics & More



Supporting Information

ABSTRACT: Selective activation of renewable carboxylic acids on promoted molybdenum oxides to form alcohols and aldehydes is reported. A combination of reaction kinetics, temperature-programmed reduction (TPR), and X-ray photoelectron spectroscopy (XPS) reveals that the activity scales with the concentration of Mo<sup>5+</sup> active sites and is a strong function of surface hydrogen coverage. The addition of a very small loading (0.05 wt %) of Pt drastically increases rates of selective deoxygenation at lower temperatures (<350 °C) but diminishes rates at elevated temperatures due to over-reduction of the support. Here, it is reported that the incorporation of Pt clusters on MoO<sub>3</sub> decreases the apparent activation barrier for acid conversion by over 32 kJ/mol, which highlights the significant role of site regeneration facilitated by hydrogen splitting and spillover. Our findings suggest that the rate-determining step for converting pentanoic acid shifts upon introducing Pt clusters from formation/regeneration of oxygen vacancies to H addition to the carbonyl carbon.



**KEYWORDS:** carboxylic acid, hydrodeoxygenation (HDO), molybdenum oxide (MoO<sub>3</sub>), metal oxides, redox chemistry, biomass conversion, hydrogen spillover, oxygen vacancies

#### 1. INTRODUCTION

The reduction of carboxylic acids to form alcohols and aldehydes is a highly desirable process for producing fuels and commodity chemicals. One of the most well-known examples of this chemistry is the selective conversion of acetic acid to form ethanol, an essential commodity feedstock used as an additive in the food and fuel industries. Another example is the selective deoxygenation of long-chain fatty acids and triglycerides, with the potential to produce surfactants. Carboxylic acids containing five carbon atoms, such as levulinic acid and pentanoic acid (PA), are particularly interesting feedstocks for producing commodity chemicals obtained from renewable organic materials.

Typical platform chemicals in biomass upgrading include carboxylic acids, sugar alcohols, and furanic compounds. Lignocellulosic biomass usually contains more than 50 wt % of sugars that could be upgraded to valuable platform molecules. These sugars in aqueous solutions can be dehydrated to yield hydroxymethylfurfural (HMF), levulinic acid (LA), and furfural (FAL); all of them have enormous potential for the production of high-value chemicals, fuels, and polymers. LA can be obtained from fructose through the hydrolysis of HMF under acidic aqueous conditions. This acid in an aqueous-phase solution can also be converted to  $\gamma$ -valerolactone (GVL), which undergoes either ring opening to

produce a mixture of unsaturated carboxylic acids  $^{4,8-12}$  or ketonic decarboxylation to generate large symmetrical ketones.  $^{13,14}$ 

The most traditional chemical pathways for upgrading carboxylic acids into more desirable products are coupling reactions to form ketones and decarboxylation/decarbonylation reactions to produce non-oxygenated hydrocarbons (alkanes and alkenes). However, the low reactivity of carboxylic acids compared to the high reactivity of alkenes (at reaction conditions) often leads to rapid oligomerization, ultimately resulting in coke formation and subsequent catalyst deactivation. Furthermore, the production of shorter-length hydrocarbon chains and  $\rm CO_2/CO$  as a byproduct is one of the main drawbacks of carboxylic acid upgrading via decarboxylation/decarbonylation. An alternative pathway is carboxylic acid reduction via selective hydrodeoxygenation (HDO), preserving C–C bonds without disturbing other chemical functionalities.

 Received:
 March 18, 2022

 Revised:
 April 26, 2022

 Published:
 May 12, 2022





Several catalysts have been proposed for the deoxygenation of acids via the formation of aldehydes and alcohols. However, most of them rely on noble metals that are highly active for hydrogenation/dehydrogenation reactions, requiring high hydrogen pressures to limit rapid coke formation and shifting product distributions to fully saturated analogues. Therefore, there is a need to develop an efficient and selective heterogeneous catalyst for carboxylic acid hydrodeoxygenation chemistry while minimizing side reactions such as coke formation, cracking reactions, and double-bond saturation associated with most metals.

As an alternative to high-pressure metal catalysts, highly oxophilic materials can reduce carboxylic acids to aldehydes. Even though these catalysts also favor coupling reactions via ketonization, fine-tuning surface conditions could inhibit these side reactions. The reduction with highly oxophilic supports carries the advantage of selective activation of the acid functional group without disturbances to other functional groups or shortening the hydrocarbon chain length. These two features are of particular importance to forming multifunctional products from carboxylic acids (e.g., C-5).

Recently, Prasomsri et al. showed that molybdenum oxide  $(MoO_3)$  could perform hydrodeoxygenation selectively on aldehydes and alcohols, forming unsaturated products at low  $H_2$  pressures. The reaction was proposed to occur at the surface via a reverse Mars-van Krevelen-type mechanism, where the oxygen atom from the reactants is abstracted by the lattice terminal oxygen vacancy, restoring the initial surface structure. Hydrogen was used as a reducing agent to regenerate the oxygen vacancies, removing oxygen as  $H_2O.^{20-22}$ 

Although partially reduced MoO<sub>3</sub> has been proven to selectively deoxygenate ketones and alcohols via HDO, reducing more challenging molecules such as long carbon chain carboxylic acids, to the best of our knowledge, has not yet been explored. Since MoO<sub>3</sub> demonstrates low relative rates for the hydrogenation of carbon—carbon double bonds, the possibility for selective conversion of unsaturated acids to highly valuable dienes could exist if selective acid deoxygenation chemistry over these catalysts was established. The intriguing affinity to selectively cleave C—O bonds over MoO<sub>3</sub> surfaces without subsequent hydrogenation of formed products makes this an excellent material to explore for selective acid reduction

Here, we report the promising activity of the  $MoO_3$  catalyst for the selective conversion of PA to pentanaldehyde (PAL) under atmospheric hydrogen pressure. The reducibility of  $MoO_3$  is known to require high temperatures; therefore, the addition of very low loadings (0.05 wt %) of Pt metal clusters to promote  $H_2$  dissociation and spillover is explored to enhance deoxygenation while exploring consequential impacts on product selectivity. We reveal that this low loading facilitates low-temperature activity of the catalyst while minimizing undesirable side reactions that may occur on the metal directly.

The results reported here demonstrated that  $MoO_3$  and  $Pt/MoO_3$  are promising catalysts for the selective reduction of carboxylic acids to aldehydes, exhibiting trade-offs between the rate and selectivity as the temperature increases. X-ray photoelectron spectroscopy (XPS) was used to investigate the distribution of different oxidation states on the surface during the partial reduction of  $MoO_3$  and 0.05 wt %  $Pt/MoO_3$  catalysts to identify the active species responsible for the selective conversion. These were complemented with density

functional theory (DFT) computational analysis that illustrates the complex transition state involved and the critical importance of surface hydrogen coverage on net reaction rates. The key role of products on the inhibition of sequential reactions of the formed products is also revealed, enabling promising selectivity to singularly deoxygenated products at elevated conversions.

### 2. EXPERIMENTAL SECTION

- **2.1. Chemical and Catalyst Materials.** PA (99%, Sigma-Aldrich) was used as a feed with no further purification.  $\rm H_2$  (99.999%, Airgas), He (99.999%, Airgas),  $\rm N_2$  (99.998%, Airgas), and air (Ultra zero, Airgas) were used in the reaction experiments and characterization techniques. Commercial molybdenum(VI) oxide,  $\rm MoO_3$  (>99.5 wt %), was purchased from Alfa Aesar and molybdenum(IV) oxide from sigma aldrich ( $\rm MoO_2$ , 99%). The catalyst was mixed with acidwashed glass beads (50–70 US sieve, Sigma).
- **2.2. Catalyst Synthesis.** The 0.05 wt % Pt/MoO<sub>3</sub> catalyst was prepared by the incipient wetness impregnation method. For a batch of 10 g of the supported catalyst, a 2 mL aqueous solution with 10 mg of tetraammineplatinum(II) nitrate (99.99%, 50% Pt, Alfa Aesar) was added dropwise to the support. Upon completion of the previous step, the sample was dried at 80 °C for 12 h and calcined at 600 °C (ramp rate 10 °C/min) for 3 h under air flow (100 mL/min). Commercial MoO<sub>3</sub> was calcined under identical conditions. Before catalytic testing, the catalyst powders were pelletized and sieved to yield pellet sizes from 90 to 125  $\mu$ m (120–170 US sieve).
- **2.3. Kinetic Measurements.** The catalytic reaction experiments were conducted in a vapor-phase packed-bed flow reactor system at atmospheric pressure. A quartz tube of 0.64 cm o.d. was used as a reactor, placed in a vertical tube furnace (Thermcraft Inc., 1200 W/115 V). The reactor tube was connected to an inlet gas line at the top and an outlet gas line at the bottom. The MoO3 catalyst bed was mixed with inert, acid-washed glass beads, packed between two layers of quartz wool inside the reactor, and situated in the furnace center. The mass of catalyst used was 10 mg, except where otherwise specified. The catalyst was reduced by flowing 100 sccm of H<sub>2</sub> through a quartz tube for 1 h at 400 °C. The liquid reactant was fed into the reactor via a syringe pump (KD Scientific) and vaporized (at 92-100 °C) before entering the reactor. PA was mixed with heptane to avoid corrosion in the syringe and needle. The vaporized reactant was mixed with H<sub>2</sub> or  $H_2/He$  gas at the inlet of the reactor.

Each reaction experiment was carried out at 280–400 °C and atmospheric pressure. The outlet stream of the reactor was heated up to 250 °C to prevent any condensation of effluents. The products were quantified via an online gas chromatography (GC) system, Agilent 6890, equipped with a flame ionization detector (FID) using an HP-INNOWAX column (Agilent, 60 m × 0.32 mm i.d. × 0.5  $\mu$ m). The injection port and FID detector were heated up to a temperature of 250 °C. Product identification was analyzed by using a gas chromatography system, Shimadzu QP-2010 GC–MS. The standard compound of each product was used to determine the retention time, and they were quantified using relative response factors estimated based on the effective carbon number (ECN).

The reactions were run without corruptions to measured rates due to external mass transfer limitations, as determined by a common experimental test where the partial pressure of the reactants and W/F ratio remain constant while the reactant flow and catalyst mass are both doubled. This test allows higher velocity at the external surface while keeping the catalyst-reactant contact time constant. Thus, if changes in conversion are observed, the apparent rate of reaction is affected by the rate of external mass transfer. The conversion should be identical in the absence of mass transfer limitations (Table S2).

**2.4. Pulse Reaction Experiments.** The role of hydrogen was investigated by a micro-pulse reactor using helium as a carrier gas, as shown in Figure S9.<sup>24</sup> The pelletized catalyst (10 mg) was mixed with glass beads and packed in a quartz tube of 0.64 cm o.d., used as a reactor. Before the reaction, the catalyst was reduced by flowing 100 sccm of  $H_2$  through a quartz tube for 1 h at 400 °C. The size of the loop was 1 mL. PA was diluted with helium or hydrogen in a 1 mL sample loop and then sent over the catalyst bed. During the period between continuous pulses, the catalyst was exposed to helium flow. The outlet stream of the reactor was heated up to 250 °C to prevent any condensation of effluents. The products were quantified via an online GC system equipped with a FID, Agilent 6890, using an HP-INNOWAX column (Agilent, 60 m  $\times$  0.32 mm i.d.  $\times$  0.5  $\mu$ m).

For oxygen vacancy characterization, the same micro-pulse reactor was connected to an atmospheric-pressure gas analyzer (MKS Cirrus 2) to quantify the oxygen uptake on the oxygen vacancies under conditions similar to those described above for the kinetics and pulse reaciton experiments. The catalyst was pre-reduced by flowing 100 sccm of  $\rm H_2$  through a quartz tube for 1 h at 400 °C. The catalyst was exposed to helium gas at 350 °C for 2 h to remove residual hydrogen. A 5 vol %  $\rm O_2/He$  gas blend was pulsed over the catalyst sample until the oxygen saturation level was reached. The oxygen chemisorption was carried out at 350 °C. The size of the loop was 1 mL. The same procedure was carried out for both the MoO<sub>3</sub> and the 0.05 wt % Pt/MoO<sub>3</sub> catalysts.

2.5. Catalyst Characterization. 2.5.1. X-ray Photoelectron Spectroscopy (XPS). The surface analysis was conducted on a PHI 5800 ESCA multi-technique system equipped with a standard aluminum (Al) kα X-ray source (1486.6 eV) and a hemispherical analyzer. The X-ray source was operated at 300 W (15 kV and 20 mA). Survey spectra (0-1400 eV) were collected with a pass energy of 187.85 eV. The core-level spectra of C (1s), O (1s), Mo (3d), and Pt (4f) were measured using a pass energy of 58.70 eV. The binding energy values were referenced to the C (1s) peak at 284.8 eV. The core-level peaks were analyzed by PHI MultiPak (Version 9.5). All the catalysts were reduced at 400 °C under a hydrogen flow (100 mL/min) for 1 h before XPS analysis. A sample transfer vessel (PHI Model 04-110) was used to transfer the ex situ reduced samples from a glove bag to the XPS chamber to avoid exposure to air. The samples were mounted on sample stubs using a double-sided conductive carbon tape. The surface composition was estimated from the integrated intensities and corrected by atomic sensitivity factors.

2.5.2. Temperature-Programmed Reduction (TPR). The reduction profiles of the catalysts were measured by using a house-built system. The TPR experiments were carried out in a 0.64 cm o.d. quartz tube packed with 50 mg of the catalyst under a 5 vol %  $\rm H_2$  in argon (Ar) with a total flow rate of 15 sccm. The temperature was increased to 1000 °C at a ramp rate of 10 °C/min and held at 1000 °C for 30 min. Hydrogen

consumption was monitored as a function of temperature using an online SRI 110 thermal conductivity detector (TCD). A cold trap that mixes isopropyl alcohol and liquid nitrogen was used to condense the water evolved in the experiment before entering the TCD.

In addition, TPR was also performed in a Netzsch STA 449F1 equipped with a pin thermocouple and a Netzsch nanobalance. Outlet gases were measured using an Aeölos quadrupole mass spectrometer (QMS 403 C), scanning each mass from 2 to 20 amu to monitor the evolution of  $\rm H_2O$  (m/z=18) and consumption of  $\rm H_2$  (m/z=2). The temperature ramp was from room temperature to 550 °C with a rate of 2 °C/min. The mass of the catalyst used for this analysis was about 50 mg.

2.5.3. Scanning Transmission Electron Microscopy. STEM was performed on a JEOL Grand ARM at UC Irvine operated at 300 kV. STEM was used to obtain a rough estimation of Pt particle size distribution. A lacey Formvar film with the lacey structure enforced by a heavy carbon coating was utilized to load the sample (lacey Formvar/carbon, 300 mesh, copper grid hole size:  $63~\mu m$ ). The samples were directly loaded to the grid after being introduced by dry loading, where two silica slides break down the samples. Compressed air was used to remove the excess loose particles.

2.5.4. Carbon Monoxide Probe Molecule Infrared Spectroscopy (CO-FTIR). In situ DRIFTS experiments were performed in a high-temperature reaction cell (Harrick Scientific) equipped with ZnSe windows. The in situ cell was mounted inside a Praying Mantis diffuse reflectance accessory (Harrick Scientific) paired with a Thermo Scientific Nicolet iS10 FTIR spectrometer equipped with a HgCdTe (MCT) detector. Spectra were collected in absorbance units with a resolution of 4 cm $^{-1}$  by merging between 64 and 256 individual scans to minimize spectral noise. Measurements were made while purging the FTIR and Praying Mantis unit with dry  $\rm N_2$  to minimize atmospheric gas interference with the beam path.

In a typical experiment, ~50 mg of the catalyst was loaded atop a bed of inert SiO<sub>2</sub> (US Nano, 20-30 nm) to reduce overall catalyst consumption. The catalyst was then oxidized at 250 °C for 1 h by ramping at 10 °C/min in a flow of pure O<sub>2</sub> (Airgas, 99.999%) at 30 sccm. After cooling in O<sub>2</sub> flow to 30 °C, the catalyst was then purged in Ar (Airgas, 99.999%) at 50 sccm for 10 min, after which a background scan was taken. Then, the catalyst was ramped to 150 °C at 10 °C/min. Once the catalyst reached 150 °C, the atmosphere was switched to 10% CO/Ar (Airgas) at 50 sccm and held at 150 °C for 30 min. The catalyst was then cooled down to 30 °C in 10% CO/ Ar before purging with Ar at 50 sccm for 10 min to collect the final spectrum of adsorbed CO. This pretreatment was found to result in the great CO adsorption onto the sample as both oxidation in pure O2 and reduction in pure H2 led to major and complete suppression, respectively, of CO adsorption.

2.5.5. BET Surface Area. The Brunauer, Emmet, and Teller (BET) surface area was calculated from the isotherms measured with a Micromeritics ASAP 2020. Approximately 2 g of each catalyst was pretreated at 400 °C under vacuum for 1.5 h prior to the adsorption analysis. The isotherms were measured at 77 K using nitrogen as the adsorptive. The BET surface area was calculated using isotherm data in the relative pressure range of  $0.05 < P/P_0 < 0.3$ .

**2.6. DFT Calculations.** The  $\alpha$ -MoO<sub>3</sub> surface was modeled using a three-dimensional periodic bulk supercell of (4  $\times$  1  $\times$ 

4) separated by an 18 Å vacuum region. The bottom Y layers of MoO<sub>3</sub> were fixed at their bulk positions, while the top Y layers were fully relaxed. DFT calculations were carried out using the VASP package.<sup>25</sup> The Perdew-Burke-Ernzerhof generalized gradient approximation exchange-correlation potential (PBE-GGA) was used,<sup>26</sup> and the electron-core interactions were treated in the projector augmented wave (PAW) method.<sup>27,28</sup> Structures were optimized until the atomic forces were smaller than 0.02 eV Å-1 with a kinetic cutoff energy of 400 eV. The van der Waals interactions were considered using the DFT-D3 semiempirical method.<sup>29</sup> Transition state structures and energies were determined using the climbing image nudged elastic band<sup>30,31</sup> and dimer methods.<sup>32</sup> The surface Brillouin zone was sampled with a single k point at Gamma. The adsorption energy  $(E_{ad})$  of the adsorbate was calculated using the equation below:

$$E_{\rm ad} = E_{\rm adsorbate-surface} - (E_{\rm adsorbate} + E_{\rm surface})$$

## 3. RESULTS AND DISCUSSION

**3.1. PA Conversion over MoO<sub>3</sub> Catalysts.** PA conversion over MoO<sub>3</sub> catalysts was evaluated at different temperatures in a fixed-bed flow reactor under atmospheric hydrogen pressure. The conversion and product distributions are shown in Figure 1. All conversions and rates reported here

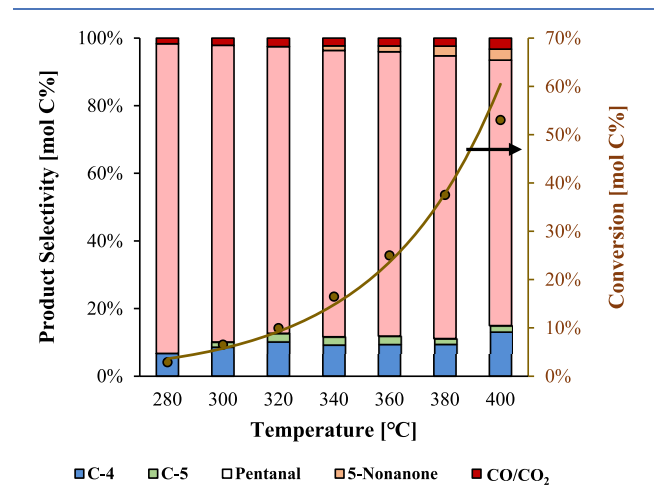


**Figure 1.** Activity for HDO of PA and product selectivity distribution for PA conversion at different reaction temperatures over MoO<sub>3</sub>. Reaction conditions: Flow of H<sub>2</sub> = 30 mL/min,  $P_{\text{Total}}$  = 1 atm, TOS = 0 min, and W/F = 0.11  $g_{\text{cat}}$ /mL·h. The catalyst was previously reduced under H<sub>2</sub> flow (100 mL/min) at 400 °C for 1 h.

were obtained after extrapolating rates to initial time on stream (TOS) to mitigate any effects of catalyst deactivation on reported rates. Under the wide temperature range studied, conversion of PA over MoO<sub>3</sub> exhibits very high selectivity to pentanal (PAL > 80%). Moreover, low selectivities to decarbonylation and C–O hydrogenolysis products were observed even at the highest conversion levels tested. The competing ketonization reaction to yield 5-nonanone was also detected in small quantities at higher reaction temperatures. Alcohols are not thermodynamically favored at the most elevated reaction temperatures tested. However, rapid dehydration to yield C-5 hydrocarbons would be expected if they were formed in equilibrium quantities. This suggests that subsequent hydrogenation of the generated products is

kinetically unfavorable under the wide range of conditions reported here. Given the well-documented potential of MoO<sub>3</sub> catalysts for the deoxygenation of aldehydes, this selectivity could potentially arise via inhibition of subsequent aldehyde readsorption due to high acid coverages.

In addition to potential competition with the acid feed to inhibit undesired side reactions such as decarbonylation, inhibition of subsequent reactions due to the presence of reaction products (e.g.,  $H_2O$ ) also appears to influence this chemistry. The role of product inhibition can be more clearly compared by evaluating product selectivity at isoconversion levels (Figure S1), revealing that decarbonylation selectivity is a more significant function of temperature than depicted at varying conversion levels in Figure 1.

Surface oxygen defects have been proposed as active sites for HDO reactions over  $MoO_3$  catalyst.  $^{33,34}$  Here, we hypothesize that the selective C–O cleavage reactions occur over these defects on the sub-stoichiometric oxide to form Mo–O bonds. These active sites can be regenerated by dissociated hydrogen to produce water. Shetty et al. showed that the rate-determining step for acetone deoxygenation to propene is the hydrogen dissociation on a stoichiometric surface, with a considerable activation barrier. However, it is noted that reduced oxygen vacancies exhibit a metallic character and likely aid in  $H_2$  dissociation once defects are created. Therefore, promoting  $MoO_3$  with small levels of a noble metal capable of fast  $H_2$  dissociation, such as Pt, should profoundly influence vacancy creation rates.

3.2. Influence of Metal Cluster (Pt) over MoO<sub>3</sub>-Based Catalysts. The addition of noble metal clusters onto MoO<sub>3</sub> is expected to facilitate H2 dissociation, leading to dissociated hydrogen spillover onto the metal oxide support to promote oxygen removal on the oxide surface. Thus, reducible oxides doped with noble metals often provide enhanced catalyst activity. 36 Sermon and Bond showed that MoO3 reduction by molecular hydrogen only takes place at appreciable rates above 400 °C. However, the catalyst reduction can occur at a lower temperature if hydrogen atoms are supplied or created at the surface.<sup>37</sup> A kinetic study of H<sub>2</sub> adsorption on MoO<sub>3</sub> showed minimal hydrogen uptake on the MoO<sub>3</sub> catalyst in the temperature range of 50-300 °C, demonstrating that the hydrogen dissociation rate on MoO<sub>3</sub> is very low under this reduction temperature range. In contrast, the same study concluded that adsorption of H<sub>2</sub> on Pt/MoO<sub>3</sub> was 190 times higher than on MoO<sub>3</sub>, which further suggests the positive role of noble metals on hydrogen dissociation and uptake on MoO<sub>3</sub>. 38,39

The TPR spectra of MoO<sub>3</sub> and 0.05 wt % Pt/MoO<sub>3</sub> samples are shown in Figure 2. MoO<sub>3</sub> does not show significant hydrogen consumption below 650 °C; only a broad H<sub>2</sub> consumption peak is observed in the 650–900 °C temperature range, attributed to the bulk MoO<sub>3</sub> reduction. In contrast, the addition of Pt clusters (0.05 wt %) on MoO<sub>3</sub> produces a significant shift in the initial reduction temperature of MoO<sub>3</sub> with considerable uptake at lower temperatures. This significant difference is ascribed to the presence of metallic Pt clusters that can easily dissociate H<sub>2</sub> and enhance the reducibility of MoO<sub>3</sub> by hydrogen spillover. In general, the reduction process of MoO<sub>3</sub> has been reported to be a two-step reduction mechanism (MoO<sub>3</sub>  $\rightarrow$  MoO<sub>2</sub>  $\rightarrow$  Mo) with the additional formation of Mo<sub>4</sub>O<sub>11</sub> in a parallel reaction (3MoO<sub>3</sub> + MoO<sub>2</sub>  $\rightarrow$  Mo<sub>4</sub>O<sub>11</sub>). <sup>40</sup>

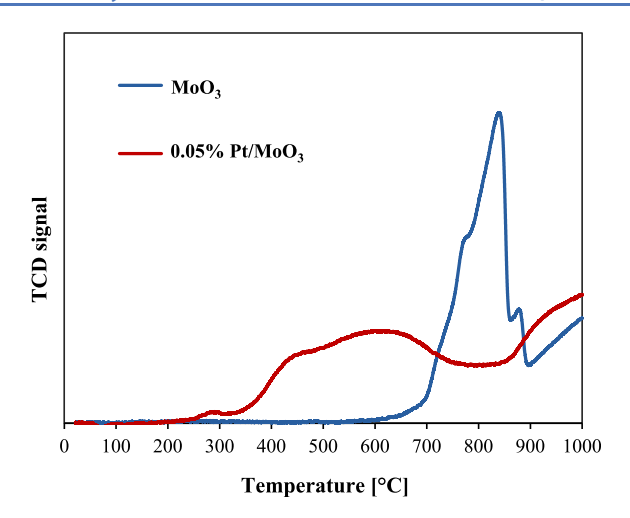


Figure 2. TPR results for MoO<sub>3</sub> and 0.05 wt % Pt/MoO<sub>3</sub> samples.

TGA-TPR was also performed to evaluate the weight loss during the reduction process; the temperature was varied from room temperature up to 550 °C in H<sub>2</sub>/Ar flow (Figure S2). The weight loss reported represents the water production by MoO<sub>3</sub> during the reduction process. For water formation, dissociated H atoms adsorbed on MoO<sub>3</sub> create hydroxyl species (–OH) with oxygen atoms located at the surface; subsequently, these are recombined to yield water molecules. For the MoO<sub>3</sub> catalyst, less than 1% weight loss was observed at 400 °C. In contrast, the 0.05 wt % Pt/MoO<sub>3</sub> catalyst exhibited 8 times more weight loss at 400 °C than MoO<sub>3</sub>. It is important to note that despite the low metallic loading, significant differences in MoO<sub>3</sub> reduction are observed upon Pt incorporation.

To characterize the Pt structure on MoO<sub>3</sub>, STEM analysis was carried out on a JEOL Grand ARM. This technique allows us to visualize if Pt exists as isolated atoms or small metallic

clusters (Figure S10). Although 0.05 wt % Pt/MoO<sub>3</sub> was synthesized via incipient impregnation, which generally promotes the formation of different cluster sizes, isolated atoms could be expected due to low Pt loading. Figure 3a,b reveals that Pt is exhibited as small clusters over  $MoO_3$ , with a wide range of particle sizes between 1.6 and 11.3 nm (Figure S11).

STEM results were coupled with probe molecule Fourier transform infrared spectroscopy (FTIR) to confirm the presence of Pt as metallic clusters. It has been shown that CO probe molecule FTIR is a useful characterization technique, 41 especially when coupled with STEM imaging, to characterize the distribution of Pt species (Pt atoms, metallic Pt<sup>0</sup> nanoparticles or clusters, or oxidized Pt clusters) on oxidesupported catalysts. The IR spectra of CO adsorbed to 0.05 and 1 wt % Pt/MoO<sub>3</sub> at room temperature following the reduction in CO at 150 °C are shown in Figure 3c,d. These materials were chosen for analysis because they were expected to represent the range of Pt loadings at different structures, such as clusters or single atoms, that could be potentially present. The primary stretch associated with adsorbed CO for both materials was centered between 2080 and 2095 cm<sup>-1</sup>. Although the literature describing CO vibrational frequency on Pt/MoO<sub>3</sub> catalysts is sparse,<sup>42</sup> we assign this feature to CO bound linearly to metallic Pt<sup>0</sup> nanoparticles or clusters based on its vibrational frequency<sup>43–46</sup> and the ability of CO to reduce Pt at temperatures as low as 400 K.47 The slight differences in peak shape and location between each material could be due to particle-size-dependent electron transfer to the support, Pt nanoparticle size, or other effects.

In addition to the primary CO stretching feature, both materials showed a small peak between 2115 and 2145 cm<sup>-1</sup>, which is more challenging to assign. The location above 2100 cm<sup>-1</sup> is indicative of CO adsorbed on cationic Pt species (i.e., Pt<sup>2+</sup>) which may be related to CO adsorption either on Pt single atoms or on oxidized Pt clusters (e.g., Pt<sub>x</sub>O<sub>y</sub>). The

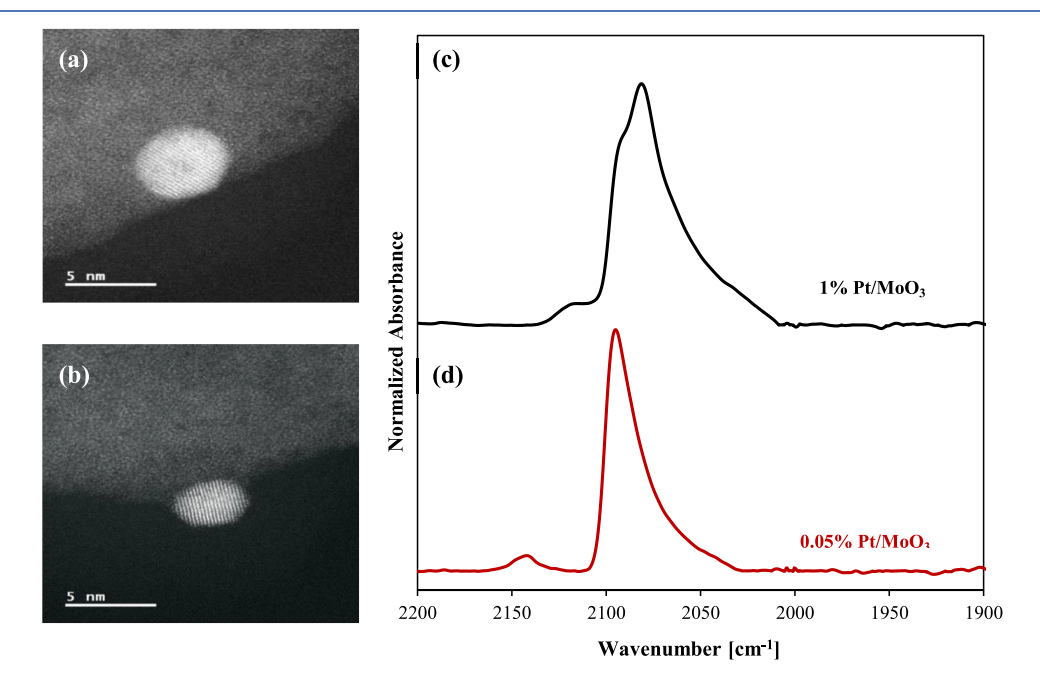


Figure 3. (a, b) STEM characterization of 0.05 wt %  $Pt/MoO_3$ . (c, d) FTIR spectra of CO adsorbed at 30 °C on two different Pt on  $MoO_3$  catalysts prepared by incipient wetness impregnation. The catalyst was pretreated at 150 °C in 10% CO/He for 30 min. (c) 1 wt %  $Pt/MoO_3$  and (d) 0.05 wt %  $Pt/MoO_3$ . Data normalized to maximum peak intensity and offset for clarity.

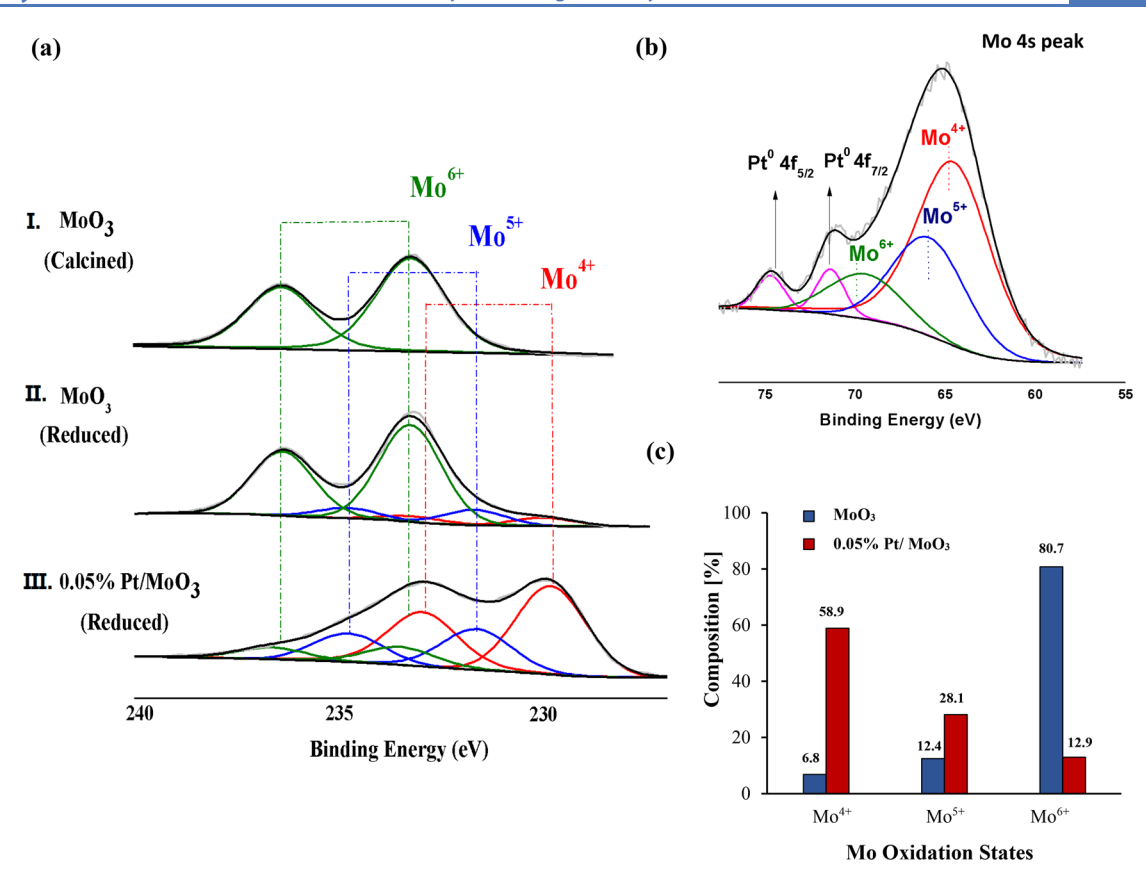


Figure 4. XPS results of  $MoO_3$  and 0.05 wt %  $Pt/MoO_3$ . (a) XPS analysis showing the Mo(3d) energy region of  $MoO_3$  calcined, reduced, and 0.05 wt %  $Pt/MoO_3$  catalysts. (b) XPS analysis showing the Pt(4f) regions for 0.05 wt %  $Pt/MoO_3$ . (c) Mo oxidation states (%) for  $MoO_3$  and 0.05 wt %  $Pt/MoO_3$ .

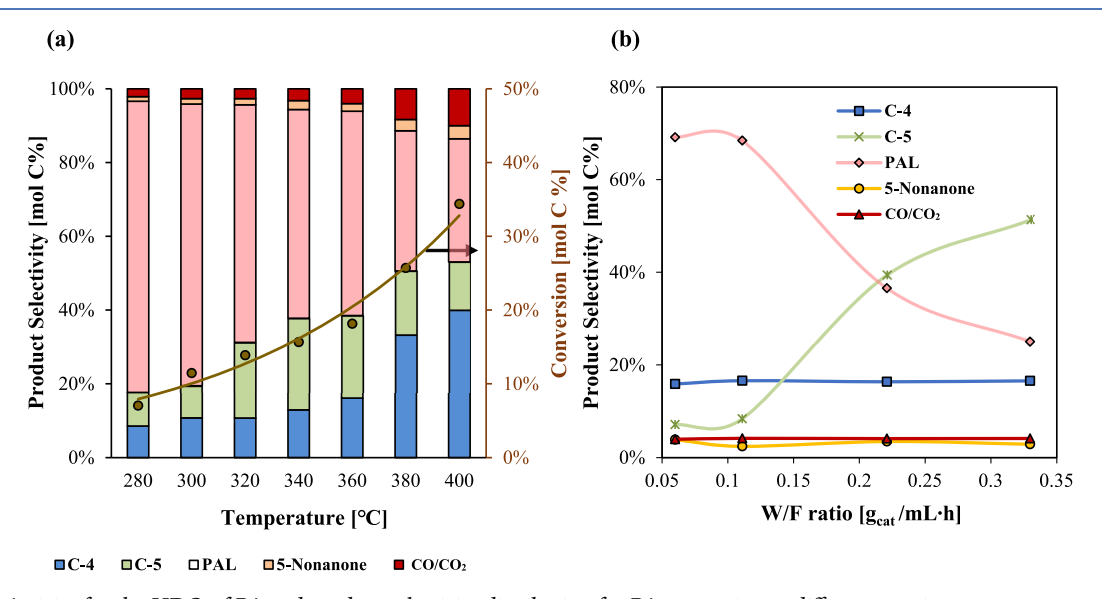


Figure 5. (a) Activity for the HDO of PA and product selectivity distribution for PA conversion at different reaction temperatures over 0.05 wt % Pt/MoO<sub>3</sub>. Reaction conditions: Flow of  $H_2 = 30$  mL/min, P = 1 atm, TOS = 0 min, and W/F = 0.11  $g_{cat}/mL \cdot h$ . (b) Dependence of product selectivity of PA conversion at various W/F using 0.05 wt % Pt/MoO<sub>3</sub> as a catalyst. Reaction conditions: Flow of  $H_2 = 30$  mL/min,  $P_{Total} = 1$  atm, and  $T_{reaction} = 350$  °C. The catalyst was previously reduced under  $H_2$  flow (100 mL/min) at 400 °C for 1 h for all cases.

latter one is more likely due to incomplete Pt reduction. This is evidenced as the relative intensity of this feature with respect to CO on the Pt<sup>0</sup> feature did not change with weight loading, as opposed to what would be expected if the feature was due to CO adsorbed to Pt single atoms. The 2115 and 2145 cm<sup>-1</sup> CO stretches make up less than 5% of the total absorbance area of

these materials, suggesting that the associated adsorption site is a minor contributor to the active Pt species.

The nature of active sites during the HDO of ketones and alcohols over  $MoO_3$  has been studied by Murugappan et al. using near-ambient pressure XPS (NAP-XPS). They showed that during the anisole feed, the transition of the oxidation

state over pre-reduced MoO<sub>3</sub> shifted from Mo<sup>5+</sup> to Mo<sup>6+</sup>. The presence of Mo<sup>4+</sup> species was also observed, which shows that some Mo sites can be over-reduced to Mo<sup>4+</sup>. However, during the HDO reaction, Mo4+ species did not correlate with reaction rates, leading them to conclude that Mo<sup>4+</sup> species were not involved in this selective HDO reaction. Thus, NAP-XPS characterization indicated that only Mo<sup>5+</sup> species are responsible for HDO activity over MoO<sub>3</sub>. Hence, the effect of oxidation states on the MoO<sub>3</sub> and 0.05 wt % Pt/MoO<sub>3</sub> catalysts was investigated using XPS. Figure 4a,b shows the XPS spectra of the Mo 3d and Pt 4f regions for three different pre-reaction samples: non-reduced MoO<sub>3</sub> and both MoO<sub>3</sub> and 0.05 wt % Pt/MoO<sub>3</sub> reduced at 400 °C in H<sub>2</sub>. XPS results clearly show a shift in the oxidation state of the Mo species after reduction in atmospheric hydrogen flow at 400 °C for 1 h. Only Mo<sup>6+</sup> species were identified in the non-reduced sample. Upon comparing the non-reduced MoO<sub>3</sub> with reduced MoO<sub>3</sub>, modest amounts of Mo<sup>4+</sup> and Mo<sup>5+</sup> were observed. The presence of Mo<sup>4+</sup> and Mo<sup>5+</sup> species in reduced samples gives evidence of surface modifications during H2 reduction.

Furthermore, XPS results show that the incorporation of Pt leads to a significant enhancement in the reduced Mo species, with most Mo existing in the Mo $^{4+}$  and Mo $^{5+}$  states. This indicates that if the rate of Mo reduction is kinetically relevant in this selective HDO reaction; the addition of small levels of the Pt dopant could accelerate the rate of carboxylic acid reduction. The corresponding binding energies for each characteristic XPS peak identified for the above samples are presented in Table S1. These results are also consistent with  $\rm O_2$  uptake measurements as described in the Experimental Section. After reduction at 400 °C followed by dilute oxygen pulses at 350 °C, 405  $\mu \rm mol/g$  O $_2$  was adsorbed on the MoO $_3$  catalyst, but 1495  $\mu \rm mol/g$  O $_2$  was adsorbed on the 0.05 wt % Pt/MoO $_3$  catalyst, further highlighting the increased concentration of vacancies after reduction in the presence of Pt.

**3.3.** Catalytic Activity for HDO Using a Promoted MoO<sub>3</sub> Catalyst. The promoting effect of small Pt clusters in the conversion of PA via HDO was investigated under the same reduction and reaction conditions as MoO<sub>3</sub> catalysis. Figure 5a shows the product selectivity of PA conversion as a function of temperature. The presence of small Pt clusters exhibits significant changes in the product distribution as a function of temperature. Here, the results show that at a higher temperature, 0.05 wt % Pt/MoO<sub>3</sub> increases the conversion toward decarboxylation (C-4) products. However, the selectivity to PAL over Pt/MoO<sub>3</sub> improves at lower temperatures (Figure 5a). This can be explained by both less-severe over-reduction of the MoO<sub>3</sub> surface under more mild reaction conditions and less nonselective chemistry promoted by the Pt metal at lower temperatures.

To understand the temperature dependence of the selectivity on 0.05 wt % Pt/MoO<sub>3</sub>, a set of experiments were conducted at different temperatures but at similar conversion levels (Figure S3). These experiments confirm that at high temperatures, the decarbonylation (C-4) reaction becomes much more prominent, as expected, due to the presence of Pt clusters. The product distribution was also studied at different contact times (W/F); Figure 5b shows that at lower W/F, high selectivity to PAL (69%) is observed with low C-5 product selectivity (7%). However, at high contact times, a shift of selectivity is observed, and the dominant product of the reaction became C-5 compounds (51% selectivity). Thus, the pentanal selectivity over 0.05 wt % Pt/MoO<sub>3</sub> was affected

when varying the conversion from 3 to 52%, suggesting that PA conversion over MoO<sub>3</sub> follows a series of sequential steps, where HDO of PA is converted to pentanal, which consecutively undergoes HDO reaction to generate C-5 products. Furthermore, the negative impact on aldehyde production at higher Pt loading on MoO<sub>3</sub> is shown in Figure S4, where higher rates of decarboxylation/decarbonylation and other side reactions are observed as Pt loading increases. Comparable trends have been observed for similar deoxygenation chemistry involving metals and reducible oxides. 48

The trade-off associated with ultra-low Pt loadings (0.05 wt %) on PA hydrodeoxygenation vs over-reduction of the surface is shown in Figure 6. The rate of PA consumption clearly

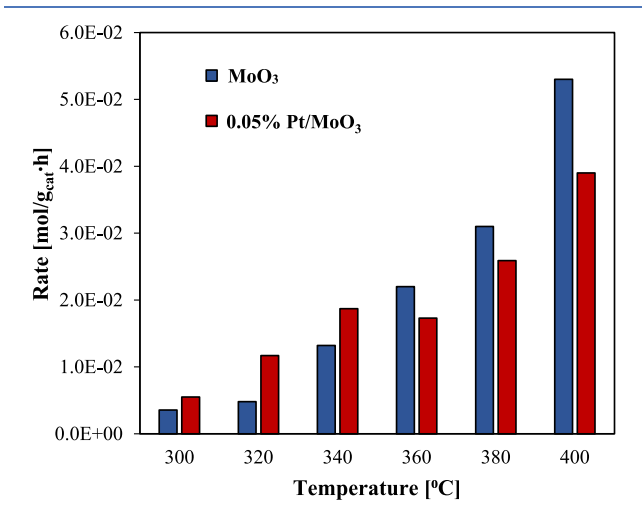


**Figure 6.** Rate of consumption of PA for both MoO<sub>3</sub> and 0.05 wt % Pt/MoO<sub>3</sub> in the temperature range 300–400 °C. Reaction conditions: Flow of  $\rm H_2 = 30~mL/min$ , TOS = 0 min,  $P_{\rm Total} = 1$  atm and W/F = 0.11  $\rm g_{cat}/mL\cdot h$ . The catalyst was previously reduced under  $\rm H_2$  flow (100 mL/min) at 400 °C for 1 h for all cases.

increases at lower temperatures when a small loading of Pt (0.05 wt %) is added. This increase in activity can be explained by XPS results, where a higher presence of Mo<sup>4+</sup> (52%) and Mo<sup>5+</sup>(16%) was observed after the reduction process (Figure 4c). In contrast, at reaction temperatures higher than 360 °C, the catalytic activity of 0.05% Pt/MoO<sub>3</sub> decreased, suggesting that during the oxidation—reduction cycle, some undercoordinated sites have been over-reduced to lower oxidation states (Mo<sup>4+</sup>). These results indicate that the benefits in deoxygenation rate that are observed upon the incorporation of small Pt loadings at lower temperatures (<350 °C) could be due to the generation of more Mo<sup>5+</sup> surface species. However, these benefits are no longer present at elevated temperatures, where over-reduction of the metal oxide catalyst (MoO<sub>3-x</sub>) can occur

Similar behavior is observed when  $MoO_3$  is over-reduced for longer times or at higher temperatures. Figure S12 shows that with a more prolonged reduction time (3 h),  $MoO_3$  exhibits a lower selectivity to pentanal. The same trend is observed when the reduction temperature is increased up to 450 °C. Figure S13 shows that with higher reduction temperatures (400–500 °C), the overall activity decreases. Thus, more severe reduction conditions appear to result in the unavoidable creation of less active  $Mo^{4+}$  species.

To investigate the effect of the total reduction of Mo species from  $Mo^{6+}$  and  $Mo^{5+}$  to  $Mo^{4+}$  on this hydrodeoxygenation

chemistry, commercial  $MoO_2$  was used as a catalyst to evaluate the activity under the same reaction conditions as the  $MoO_3$  catalyst. A commercial  $MoO_2$  is prepared by reducing  $MoO_3$  in dry hydrogen at  $500~^{\circ}$ C. Figure S14 shows a higher conversion rate ( $mol/h\cdot g_{cat}$ ) for  $MoO_3$  than for  $MoO_2$ . However, due to the difference in surface area of these materials, a comparison rate per surface area is also shown in Figure S14, where the low catalytic activity for  $MoO_2$  is evident. Thus, these results indicate that a partial reduction of Mo species at the surface is needed to maintain high deoxygenation rates, and the formation of  $MoO_2$  during reaction conditions due to overreduction leads to an inactive phase, in agreement with prior proposals.  $^{34}$ 

The influence of these species on catalyst stability was investigated at intermediate temperatures (350 °C), where the conversion per gram of 0.05 wt % Pt/MoO<sub>3</sub> is comparable to the conversion per gram of MoO<sub>3</sub>. Figure S16a,b shows that both catalysts exhibit similar deactivation trends when evaluated at similar initial conversion levels, with slightly enhanced deactivation rates observed for the Pt-doped catalyst. While contrasting deactivation rates with those observed over MoO<sub>3</sub> under identical temperatures with m-cresol,<sup>49</sup> it is evident that both catalysts in the current study exhibit slightly higher stability as a function of time, implying low coke formation rates for aliphatic acids when compared to aromatic oxygenate compounds.

The results presented thus far highlight the relevant role of oxygen vacancies in the HDO reaction of PA over MoO<sub>3</sub> and illustrate how the creation of these sites can be accelerated by adding a small amount of metal dopants under mild conditions (<350 °C). To demonstrate the role of Pt in this chemistry at lower temperatures, experiments were carried out over MoO<sub>3</sub> and 0.05 wt % Pt/MoO<sub>3</sub> using the identical catalyst mass but different reaction temperatures to achieve isoconversion. Figure 7 reveals that the addition of 0.05 wt % Pt reduces the temperature required by 40 °C to achieve a similar conversion level (9%) while maintaining high selectivity to pentanal. It is noted that even under these mild conditions,

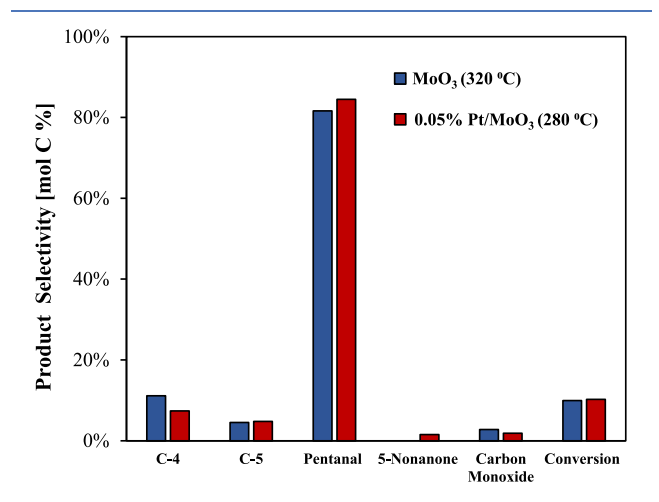


Figure 7. Product distribution at the same conversion levels for  $MoO_3$  (320 °C) and 0.05 wt % Pt/MoO<sub>3</sub> (280 °C). Comparison of product distribution measured at the same conversion levels with different temperatures for both catalysts. Conversion: ~9%. Reaction conditions: Flow of  $H_2 = 30$  mL/min, TOS = 0 min, W/F = 0.11  $g_{cat}/mL\cdot h$ , and  $P_{Total} = 1$  atm. The catalyst was previously reduced under  $H_2$  flow (100 mL/min)) at 400 °C for 1 h for all cases.

some selectivity is lost due to the presence of trace Pt levels, as evidenced by the slightly higher yields to fully deoxygenated products. Nonetheless, this significant shift in the rate at low temperatures highlights the critical role that hydrogen dissociation plays in this reaction. Hence, similar steady-state levels of oxygen vacancies could be obtained at lower temperatures by tuning the addition of the Pt metal. In this regard, we hypothesize that the effect of the Pt clusters increases the concentration of OH groups and reduction rate of MoO<sub>3</sub> catalysts, resulting in enhanced rates of oxygen defect formation and potentially higher H surface coverage under reaction conditions (Figure 8a).

The energetic barriers for the conversion of PA were measured for both catalysts to provide further evidence of the enhancing effect of the metal oxide surface doped with Pt (Figure 8b). As a result, the apparent activation energy observed for MoO<sub>3</sub> (72 kJ/mol) is significantly higher than the 0.05 wt % Pt/MoO<sub>3</sub> (40 kJ/mol). Therefore, the incorporation of Pt clusters as a promoter of hydrogen dissociation reduced the kinetic barrier by 32 kJ/mol, which suggests that the ratelimiting step could be either the formation/regeneration of oxygen vacancies or a surface reaction with a strong correlation between hydrogen surface coverages on the stabilization of kinetically relevant transition states. These apparent activation energies were calculated under a slightly negative-order kinetic regime (-0.19) due to the high binding energy of acid over undercoordinated MoO<sub>3-x</sub> sites (Figure S5). The slightly negative order with respect to acid suggests that the acid is impeding the overall rate by negatively impacting hydrogen dissociation, spillover across the surface, or vacancy regener-

3.4. DFT Study for PA over MoO<sub>3</sub>. Here, we also explored the energetic barriers for the conversion of PA to PAL by performing computational calculations on reduced MoO<sub>3</sub> (010). Mei et al. showed that the creation of oxygen vacancies is more favorable at the single-coordinate terminal oxygen than both two-coordinate asymmetric and three-coordinate symmetric bridging oxygen atoms due to the lower formation energy.<sup>33</sup> Therefore, this study considered two adsorption conformation energies of PA on the  $\alpha$ -MoO<sub>3</sub> (010) surface with a single-coordinated terminal oxygen vacancy. The first adsorption conformation assumed for the conversion of PA to PAL is through the oxygen atom double-bonded to a carbonyl carbon atom (C=O), which results in the high adsorption energy of -104 kJ/mol (Figure S6a). The computed adsorption energy for the second configuration, adsorption of PA on a terminal oxygen defect through the oxygen of the hydroxyl group (-OH), is -47 kJ/mol (Figure S6b), indicating a much weaker interaction compared to the first configuration. Shetty et al. studied the hydrodeoxygenation of acetone to propylene on the  $\alpha$ -MoO<sub>3</sub> (010) catalyst. Their results indicate that dissociative hydrogen adsorption is the rate-limiting step in the catalytic cycle (170 kJ/mol).<sup>35</sup> However, as mentioned earlier, the results of our experiments reveal that Pt addition can quickly accelerate the hydrogen dissociation and oxygen vacancy formation/regeneration on MoO<sub>3</sub>.

Figure 9a shows the energetic requirements for the elementary steps involved in the formation of PAL. Following the adsorption of PA on an oxygen defect  $(O_t)$  through the hydroxyl group (-OH), a metal carboxylate intermediate (PA-H) is formed after the hydrogen atom abstraction from the hydroxyl group. This step is exothermic with a reaction energy

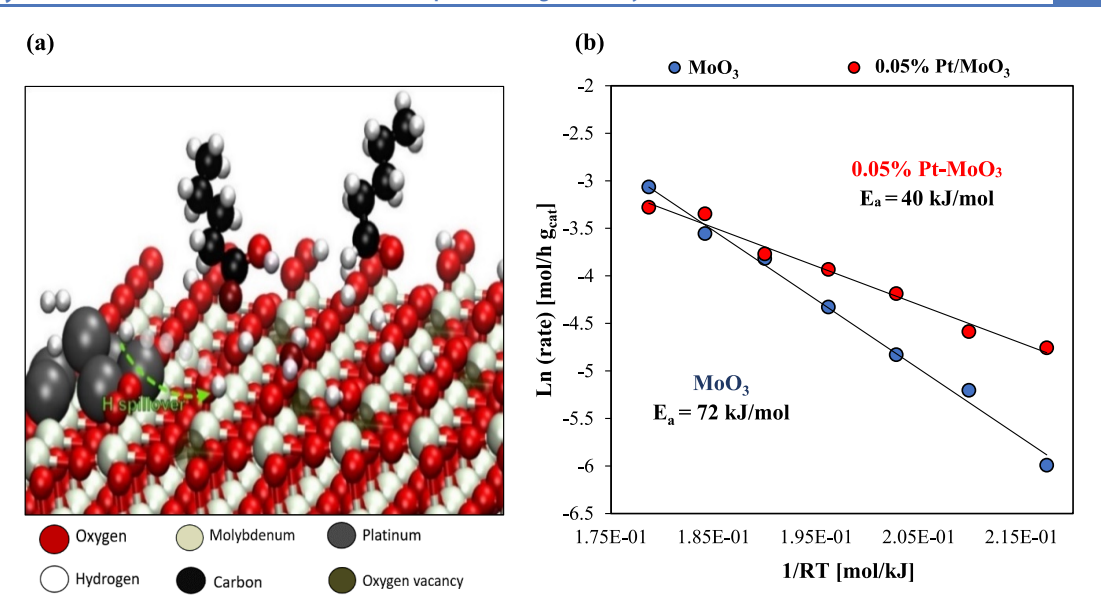


Figure 8. (a) Schematic of PA to PAL reaction over a hydrogen-covered Pt/MoO<sub>3</sub> surface. (b) Activation energy using MoO<sub>3</sub> and 0.05 wt % Pt/MoO<sub>3</sub> as a catalyst. The rate reported here is based on PA consumption. Reaction conditions: Flow of  $H_2 = 30$  mL/min, TOS = 0 min, W/F = 0.11  $g_{cat}$ /mL·h, and  $P_{Total} = 1$  atm. The catalyst was previously reduced under  $H_2$  flow (100 mL/min) at 400 °C for 1 h for all cases.

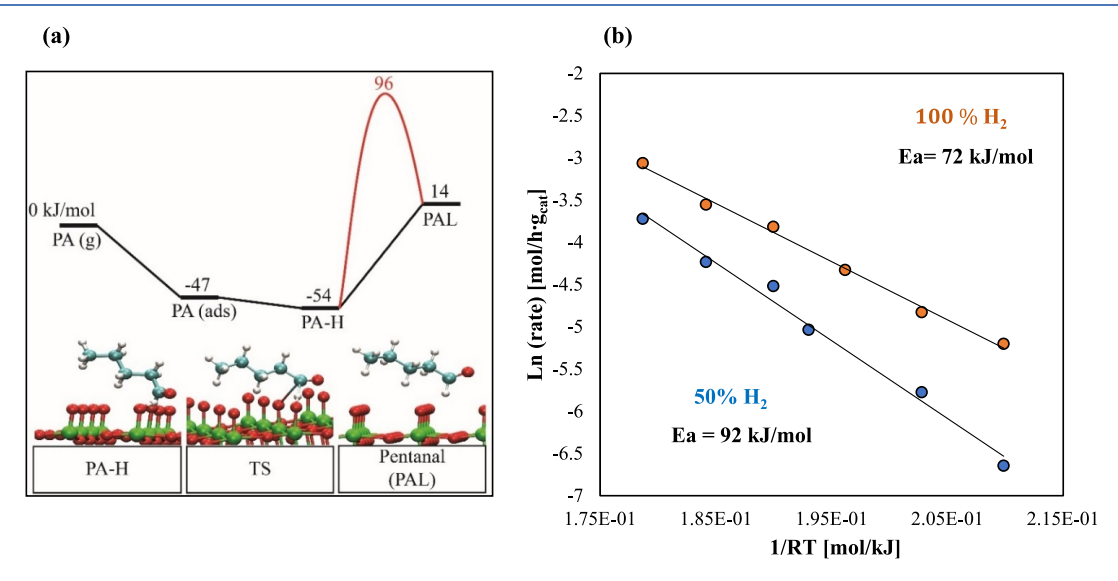


Figure 9. (a) Reaction coordinate for the formation of PAL. (b) Activation energy using MoO<sub>3</sub> as a catalyst at different partial H<sub>2</sub> pressures. The rate reported here is based on PA consumption. For all the cases, the reaction conditions were as follows:  $P_{\text{Total}} = 1$  atm, flow of H<sub>2</sub> = 30 mL/min, W/F = 0.11 g<sub>cat</sub>/mL·h, and TOS = 0 min. The catalyst was previously reduced under H<sub>2</sub> flow (100 mL/min) at 400 °C for 1 h. In the case of 50% H<sub>2</sub>, the total pressure was balanced with helium.

of -7 kJ/mol. The formation of a physisorbed PAL occurs following hydrogen-assisted deoxygenation, an endothermic step with a reaction energy of 60 kJ/mol and an apparent barrier of 96 kJ/mol. At the transition state, the bond lengths for the C-O and O-H bonds are 2.85 and 1.09 Å, respectively, indicating that the C-O bond is broken (Figure S7). These results suggest that H addition to carbonyl carbon is energetically demanding. The intermediate, transition, and final state geometries are shown in Figure 9a. All values presented were calculated at 0 K on a pristine molybdenum oxide surface and did not account for the entropy, pressure, or coverage effects.

The theoretically computed apparent barrier for the formation of PAL over a single oxygen vacancy in the absence of residual O-H (hydrogen atom absorbed in oxygen nearby)

groups is 150 kJ/mol, which is greater than the barrier experimentally observed (72 kJ/mol) in the absence of Pt. It is worth mentioning that reaction conditions and DFT-modeled conditions are not the same; therefore, a straight comparison cannot be made. However, we hypothesize that this difference can be explained by hydrogen and hydroxyl groups at the surface under reaction conditions. To further investigate the effect of hydrogen coverage in the catalytic conversion of PA to PAL, a kinetic barrier was experimentally determined when the partial pressure of hydrogen was reduced by 50% (balance with He), maintaining the overall pressure constant. Figure 9b shows that the activation energy increases by 20 kJ/mol when the partial pressure of  $\rm H_2$  is decreased by 50%, suggesting that hydrogen coverage plays a significant role in converting PA to PAL over MoO<sub>3</sub>.

ACS Catalysis pubs.acs.org/acscatalysis Research Article

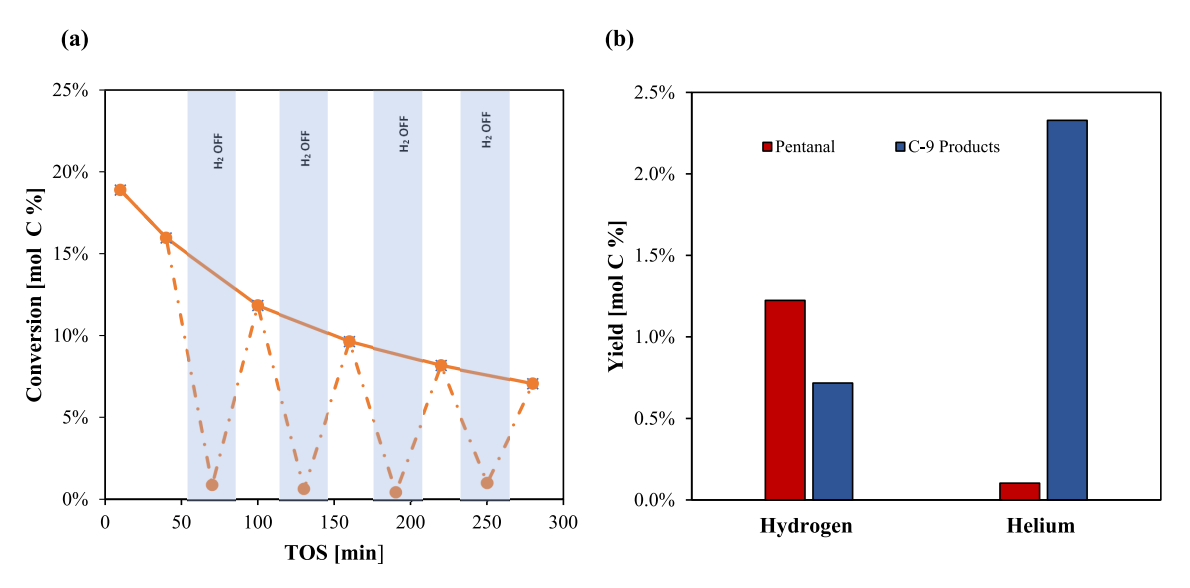


Figure 10. (a) Effect of hydrogen suppression in the conversion of PA over  $MoO_3$  in a flow system evaluated at 350 °C. The reaction conditions were as follows:  $P_{Total} = 1$  atm, flow of  $H_2 = 30$  mL/min, W/F = 0.11  $g_{cat}/mL·h$ , and TOS = 0 min. The catalyst was previously reduced under  $H_2$  flow (100 mL/min) at 400 °C. (b) Role of the hydrogen for the conversion of PA over  $MoO_3$  at 350 °C, assessed in a micro-pulse reactor. The data represented on this graph correspond to the yields after 9 pulses. The catalyst was previously reduced under  $H_2$  flow (100 mL/min) at 400 °C for 1 h for all the cases.

An alternative mechanism was tested, in which PA adsorbs through the carbonyl group at an oxygen vacancy, as shown in Figure S15, followed by C=O bond cleavage and hydrogen transfer. This proposed mechanism was investigated stepwise, showing a barrier over 300 kJ/mol for the C=O cleavage. Instead, the concerted mechanism seems more feasible; however, the intrinsic activation energy of this mechanism is 223 kJ/mol, which is significantly higher than the one presented in Figure 9a. These results suggest that, though adsorption via the carbonyl group is stronger, PA in this adsorption configuration is likely a spectator due to the high activation barrier.

3.5. Role of Intermediate Hydrogen Pulses on Acid **Conversion Chemistry.** The intriguing role of hydrogen in modifying the rate of PA conversion was investigated further by intermittently switching the carrier gas from H<sub>2</sub> to inert He during a continuous flow reaction. We note that the catalyst was initially reduced at the same conditions mentioned above, so the results obtained over the initial 40 min are identical to those reported earlier. As shown in Figure 10a, in the absence of hydrogen in the flow system, the catalytic activity of MoO<sub>3</sub> rapidly diminishes to exhibit negligible conversions (<2%). This can be explained by the suppression of vacancy regeneration in the absence of hydrogen and the decline in hydrogen coverage on the surface. However, the catalytic activity is recovered once hydrogen is reintroduced to the reactive system. These results suggest that the coverage of hydrogen plays an essential role in this chemistry, along with the surface changes occurring during the reaction.

In order to investigate this behavior further, a micro-pulse reactor technique was used as a unique tool to probe the mechanism responsible for this dynamic chemistry (Figure S9).<sup>24</sup> Small doses of carboxylic acid diluted with hydrogen or helium were introduced via a sample loop to a reduced MoO<sub>3</sub> surface, allowing us to probe the initial interactions of reactants with the catalyst surface prior to significant modifications of the catalyst surface due to coke formation and other effects induced by persistent reactant flow. Thus, this technique

decouples the acid conversion from oxygen vacancy formation/regeneration steps. Figure 10b shows that the production of PAL is favored only in the presence of hydrogen, which clearly indicates that existing OH groups on the catalyst surface are necessary for aldehyde formation. In the presence of the inert carrier, this chemistry is less pronounced, instead favoring ketone formation. While it could be proposed that H removed from the dissociated acid species upon adsorption could ultimately transfer back to form the aldehyde product, we anticipate that it would be entropically favorable for this H atom to migrate along the catalyst surface away from the reactive intermediate. This requires a significant H coverage on the surface to facilitate the removal of formed pentanal products. The small yield of pentanal observed under inert gas could be due to the presence of residual H atoms from pretreatment carried out in the hydrogen gas. Supporting this argument is the decline in activity of pentanal production in an inert gas environment with sequential pulses, as shown in Figure S8.

Our findings suggest that carboxylic acid conversion over MoO<sub>3</sub> occurs via a more complex mechanism than a simplified reverse Mars-van Krevelen mechanism, where the PA (-OH) oxygen is adsorbed on the vacancy, which is healed and subsequently converts the acid to aldehyde. The presence of nearby hydrogen coverage is a residual requirement for this chemistry to occur. As shown above, this crucial step involving the carbonyl carbon protonation is energetically demanding, as suggested by DFT calculations. A more detailed kinetic model considering the water and CO poisoning effect and hydrogen surface coverage and the effect of hydrogen on the theoretically computed barrier should provide more insights into this dynamic reaction.

#### 4. CONCLUSIONS

Here, we demonstrate that  $MoO_3$ -based catalysts are remarkably selective for the deoxygenation of carboxylic acids to aldehydes. Under mild conditions (<350 °C), dissociation of hydrogen and generation of undercoordinated

sites are slow, with overall deoxygenation rates significantly enhanced upon the addition of trace levels of Pt. The addition of only 0.05 wt % Pt leads to a significant 32 kJ/mol reduction in the activation barrier under low temperatures at the expense of deoxygenation side reactions and activity losses due to overreduction at more elevated temperatures. DFT results and experimental hydrogen coverage studies reveal that although defects on the surface are essential, persistent coverage of surface H atoms facilitates high rates of selective acid reduction. DFT analysis also indicated that hydrogen addition to the carbonyl group is an energetically demanding step. Here, we also showed that the apparent activation energy increased by 20 kJ/mol when the hydrogen partial pressure was reduced by 50%. A micro-pulse reactor was used to decouple the oxygen vacancy formation steps from carboxylic acid conversion, confirming the critical role of persistent H coverage.

#### ASSOCIATED CONTENT

## Supporting Information

The Supporting Information is available free of charge at https://pubs.acs.org/doi/10.1021/acscatal.2c01350.

Product distribution at the same conversion level for MoO<sub>3</sub>; TGA-TPR profiles for MoO<sub>3</sub> and Pt/MoO<sub>3</sub>; binding energies of Mo (3d) doublet for Mo<sup>4+</sup>, Mo<sup>5+</sup>, and Mo<sup>6+</sup> and Pt (4f) doublet for Pt<sup>0</sup>, as determined by XPS characterization; product distribution at the same conversion levels for 0.05 wt % Pt/MoO3; reaction rate and selectivity using different loadings of Pt over MoO<sub>3</sub> at 350 °C; order of reaction with respect to PA over MoO3; two different adsorptions of PA on the MoO3 defect site; transition state for the conversion of PA to PAL over the MoO<sub>3</sub> defect site; external mass transfer test; product yield for the conversion of PA over MoO<sub>3</sub> by using a micro-pulse reactor; diagram of the pulse system; STEM and BET analyses; and catalyst deactivation at different pre-reduction temperatures (PDF)

#### AUTHOR INFORMATION

#### **Corresponding Author**

Steven P. Crossley — School of Chemical, Biological and Materials Engineering, University of Oklahoma, Norman, Oklahoma 73019, United States; oorcid.org/0000-0002-1017-9839; Email: stevencrossley@ou.edu

## **Authors**

- Laura A. Gomez School of Chemical, Biological and Materials Engineering, University of Oklahoma, Norman, Oklahoma 73019, United States
- Reda Bababrik School of Chemical, Biological and Materials Engineering, University of Oklahoma, Norman, Oklahoma 73019, United States
- Mallikharjuna R. Komarneni School of Chemical, Biological and Materials Engineering, University of Oklahoma, Norman, Oklahoma 73019, United States
- Justin Marlowe Department of Chemical Engineering, University of California Santa Barbara, Santa Barbara, California 93106, United States
- Taha Salavati-fard School of Chemical, Biological and Materials Engineering, University of Oklahoma, Norman,

- Oklahoma 73019, United States; o orcid.org/0000-0002-2830-1855
- Andrew D. D'Amico School of Chemical, Biological and Materials Engineering, University of Oklahoma, Norman, Oklahoma 73019, United States
- Bin Wang School of Chemical, Biological and Materials Engineering, University of Oklahoma, Norman, Oklahoma 73019, United States; Occid.org/0000-0001-8246-1422
- Phillip Christopher Department of Chemical Engineering, University of California Santa Barbara, Santa Barbara, California 93106, United States; orcid.org/0000-0002-4898-5510

Complete contact information is available at: https://pubs.acs.org/10.1021/acscatal.2c01350

#### Notes

The authors declare no competing financial interest.

## ACKNOWLEDGMENTS

This material is based upon work supported by the National Science Foundation under Grant CAREER 1653935, whose support is gratefully acknowledged. The DFT calculations were performed using computational resources at the OU Supercomputing Center for Education & Research (OSCER) at the University of Oklahoma.

#### REFERENCES

- (1) Zhang, M.; Yao, R.; Jiang, H.; Li, G.; Chen, Y. Insights into the Mechanism of Acetic Acid Hydrogenation to Ethanol on Cu(111) Surface. *Appl. Surf. Sci.* **2017**, *412*, 342–349.
- (2) Pei, Z.-F.; Ponec, V. On the Intermediates of the Acetic Acid Reactions on Oxides: An IR Study. *Appl. Surf. Sci.* **1996**, *103*, 171–182
- (3) Chiappero, M.; Do, P. T. M.; Crossley, S.; Lobban, L. L.; Resasco, D. E. Direct Conversion of Triglycerides to Olefins and Paraffins over Noble Metal Supported Catalysts. *Fuel* **2011**, *90*, 1155–1165.
- (4) Serrano-Ruiz, J. C.; Pineda, A.; Balu, A. M.; Luque, R.; Campelo, J. M.; Romero, A. A.; Ramos-Fernández, J. M. Catalytic Transformations of Biomass-Derived Acids into Advanced Biofuels. *Catal. Today* **2012**, *195*, 162–168.
- (5) Huber, G. W.; Iborra, S.; Corma, A. Synthesis of Transportation Fuels from Biomass: Chemistry, Catalysts, and Engineering. *Chem. Rev.* **2006**, *106*, 4044–4098.
- (6) Chheda, J. N.; Huber, G. W.; Dumesic, J. A. Liquid-Phase Catalytic Processing of Biomass-Derived Oxygenated Hydrocarbons to Fuels and Chemicals. *Angew. Chem. Int. Ed.* **2007**, *46*, 7164–7183.
- (7) Climent, M. J.; Corma, A.; Iborra, S. Conversion of Biomass Platform Molecules into Fuel Additives and Liquid Hydrocarbon Fuels. *Green Chem.* **2014**, *16*, 516–547.
- (8) Serrano-Ruiz, J. C.; Dumesic, J. A. Catalytic Routes for the Conversion of Biomass into Liquid Hydrocarbon Transportation Fuels. *Energy Environ. Sci.* **2011**, *4*, 83–99.
- (9) Wright, W. R. H.; Palkovits, R. Development of Heterogeneous Catalysts for the Conversion of Levulinic Acid to  $\gamma$ -Valerolactone. ChemSusChem 2012, 5, 1657–1667.
- (10) Alonso, D. M.; Wettstein, S. G.; Dumesic, J. A. Gamma-Valerolactone, a Sustainable Platform Molecule Derived from Lignocellulosic Biomass. *Green Chem.* **2013**, *15*, 584–595.
- (11) Bond, J. Q.; Martin Alonso, D.; West, R. M.; Dumesic, J. A. γ-Valerolactone Ring-Opening and Decarboxylation over SiO2/Al2O3 in the Presence of Water. *Langmuir* **2010**, *26*, 16291–16298.
- (12) Bond, J. Q.; Alonso, D. M.; Wang, D.; West, R. M.; Dumesic, J. A. Integrated Catalytic Conversion of Gamma-Valerolactone to Liquid Alkenes for Transportation Fuels. *Science* **2010**, 327, 1110–1114.

- (13) Serrano-Ruiz, J. C.; Wang, D.; Dumesic, J. A. Catalytic Upgrading of Levulinic Acid to 5-Nonanone. *Green Chem.* **2010**, *12*, 574–577.
- (14) Pham, T. N.; Sooknoi, T.; Crossley, S. P.; Resasco, D. E. Ketonization of Carboxylic Acids: Mechanisms, Catalysts, and Implications for Biomass Conversion. *ACS Catal.* **2013**, *3*, 2456–2473.
- (15) Sitthisa, S.; Resasco, D. E. Hydrodeoxygenation of Furfural Over Supported Metal Catalysts: A Comparative Study of Cu, Pd and Ni. *Catal. Lett.* **2011**, *141*, 784–791.
- (16) Xie, J.; Duan, P.; Kaylor, N.; Yin, K.; Huang, B.; Schmidt-Rohr, K.; Davis, R. J. Deactivation of Supported Pt Catalysts during Alcohol Oxidation Elucidated by Spectroscopic and Kinetic Analyses. *ACS Catal.* **2017**, *7*, 6745–6756.
- (17) Kim, S.; Kwon, E. E.; Kim, Y. T.; Jung, S.; Kim, H. J.; Huber, G. W.; Lee, J. Recent Advances in Hydrodeoxygenation of Biomass-Derived Oxygenates over Heterogeneous Catalysts. *Green Chem.* **2019**, *21*, 3715–3743.
- (18) Pestman, R.; Koster, R. M.; Pieterse, J. A. Z.; Ponec, V. Reactions of Carboxylic Acids on Oxides: 1. Selective Hydrogenation of Acetic Acid to Acetaldehyde. *J. Catal.* 1997, 168, 255–264.
- (19) Pestman, R.; van Duijne, A.; Pieterse, J.; Ponec, V. The Formation of Ketones and Aldehydes from Carboxylic Acids, Structure-Activity Relationship for Two Competitive Reactions. *J. Mol. Catal. A-Chem.* **1995**, *103*, 175–180.
- (20) Prasomsri, T.; Nimmanwudipong, T.; Román-Leshkov, Y. Effective Hydrodeoxygenation of Biomass-Derived Oxygenates into Unsaturated Hydrocarbons by MoO3 Using Low H2 Pressures. *Energy Environ. Sci.* **2013**, *6*, 1732–1738.
- (21) Prasomsri, T.; Shetty, M.; Murugappan, K.; Román-Leshkov, Y. Insights into the Catalytic Activity and Surface Modification of MoO3 during the Hydrodeoxygenation of Lignin-Derived Model Compounds into Aromatic Hydrocarbons under Low Hydrogen Pressures. *Energy Environ. Sci.* **2014**, *7*, 2660–2669.
- (22) Shetty, M.; Murugappan, K.; Prasomsri, T.; Green, W.; Román-Leshkov, Y. Reactivity and Stability Investigation of Supported Molybdenum Oxide Catalysts for the Hydrodeoxygenation (HDO) of m-Cresol. *J. Catal.* **2015**, *331*, 86–97.
- (23) Cheng, H.; Chen, L.; Cooper, A. C.; Sha, X.; Pez, G. P. Hydrogen Spillover in the Context of Hydrogen Storage Using Solid-State Materials. *Energy Environ. Sci.* **2008**, *1*, 338–354.
- (24) Deshpande, A.; Krishnaswamy, S.; Ponnani, K. Pulsed Micro-Reactor: An Alternative to Estimating Kinetic Parameters of Non-Catalytic Gas—Solid Reactions. *Chem. Eng. Res. Des.* **2016**, *117*, 382—393.
- (25) Kresse, G.; Furthmüller, J. Efficient Iterative Schemes for Ab Initio Total-Energy Calculations Using a Plane-Wave Basis Set. *Phys. Rev. B* **1996**, *54*, 11169–11186.
- (26) Perdew, J. P.; Burke, K.; Ernzerhof, M. Generalized Gradient Approximation Made Simple [Phys. Rev. Lett. 77, 3865 (1996)]. Phys. Rev. Lett. 1997, 78, 1396.
- (27) Blöchl, P. E. Projector Augmented-Wave Method. *Phys. Rev. B* **1994**, *50*, 17953–17979.
- (28) Kresse, G.; Joubert, D. From Ultrasoft Pseudopotentials to the Projector Augmented-Wave Method. *Phys. Rev. B* **1999**, *59*, 1758.
- (29) Grimme, S.; Antony, J.; Ehrlich, S.; Krieg, H. A Consistent and Accurate Ab Initio Parametrization of Density Functional Dispersion Correction (DFT-D) for the 94 Elements H-Pu. *J. Chem. Phys.* **2010**, 132, 154104.
- (30) Henkelman, G.; Uberuaga, B. P.; Jónsson, H. A Climbing Image Nudged Elastic Band Method for Finding Saddle Points and Minimum Energy Paths. *J. Chem. Phys.* **2000**, *113*, 9901–9904.
- (31) Henkelman, G.; Jónsson, H. Improved Tangent Estimate in the Nudged Elastic Band Method for Finding Minimum Energy Paths and Saddle Points. *J. Chem. Phys.* **2000**, *113*, 9978–9985.
- (32) Henkelman, G.; Jónsson, H. A Dimer Method for Finding Saddle Points on High Dimensional Potential Surfaces Using Only First Derivatives. *J. Chem. Phys.* **1999**, *111*, 7010–7022.

- (33) Mei, D.; Karim, A. M.; Wang, Y. Density Functional Theory Study of Acetaldehyde Hydrodeoxygenation on MoO3. *J. Phys. Chem.* C 2011, 115, 8155–8164.
- (34) Murugappan, K.; Anderson, E.; Teschner, D.; Jones, T.; Skorupska, K.; Román-Leshkov, Y. Operando NAP-XPS Unveils Differences in MoO3 and Mo2C during Hydrodeoxygenation. *Nat. Catal.* **2018**, *1*, 960.
- (35) Shetty, M.; Buesser, B.; Román-Leshkov, Y.; Green, W. H. Computational Investigation on Hydrodeoxygenation (HDO) of Acetone to Propylene on  $\alpha$ -MoO3 (010) Surface. *J. Phys. Chem. C* **2017**, *121*, 17848–17855.
- (36) Ruiz Puigdollers, A.; Schlexer, P.; Tosoni, S.; Pacchioni, G. Increasing Oxide Reducibility: The Role of Metal/Oxide Interfaces in the Formation of Oxygen Vacancies. ACS Catal. 2017, 7, 6493–6513.
- (37) Sermon, P. A.; Bond, G. C. Studies of Hydrogen Spillover. Part 1.—Study of the Rate, Extent and Products of Hydrogen Spillover from Platinum to the Trioxides of Tungsten and Molybdenum. *J. Chem. Soc., Faraday Trans.* 1 1976, 72, 730–744.
- (38) Matsuda, T.; Uchijima, F.; Sakagami, H.; Takahashi, N. H2-Reduction of Pt/MoO3 to MoOx with a Large Surface Area and Its Catalytic Activities for the Conversions of Heptane and Propan-2-Ol. *Phys. Chem. Chem. Phys.* **2001**, *3*, 4430–4436.
- (39) Triwahyono, S.; Jalil, A. A.; Timmiati, S. N.; Ruslan, N. N. B.; Hattori, H. Kinetics Study of Hydrogen Adsorption over Pt/MoO3. *Appl. Catal. A: Gen.* **2010**, *372*, 103–107.
- (40) Ressler, T.; Jentoft, R.; Wienold, J.; Günter, M.; Timpe, O. In Situ XAS and XRD Studies on the Formation of Mo Suboxides during Reduction of MoO3. *J. Phys. Chem. B* **2000**, *104*, 6360–6370.
- (41) DeRita, L.; Dai, S.; Lopez-Zepeda, K.; Pham, N.; Graham, G. W.; Pan, X.; Christopher, P. Catalyst Architecture for Stable Single Atom Dispersion Enables Site-Specific Spectroscopic and Reactivity Measurements of CO Adsorbed to Pt Atoms, Oxidized Pt Clusters, and Metallic Pt Clusters on TiO2. *J. Am. Chem. Soc.* **2017**, *139*, 14150–14165.
- (42) Zhou, S.; Yang, Y.; Yin, P.; Ren, Z.; Wang, L.; Wei, M. Metal—Support Synergistic Catalysis in Pt/MoO3–x Nanorods toward Ammonia Borane Hydrolysis with Efficient Hydrogen Generation. ACS Appl. Mater. Interfaces 2022, 14, 5275–5286.
- (43) Zhang, Q.; Mo, S.; Li, J.; Sun, Y.; Zhang, M.; Chen, P.; Fu, M.; Wu, J.; Chen, L.; Ye, D. In Situ DRIFT Spectroscopy Insights into the Reaction Mechanism of CO and Toluene Co-Oxidation over Pt-Based Catalysts. *Catal. Sci. Technol.* **2019**, *9*, 4538–4551.
- (44) Mihaylov, M.; Hadjiivanov, K.; Knözinger, H. Effect of Cr and Pt Promoters on the Surface Properties of Tungstated Zirconia: FTIR Spectroscopy of Probe Molecules (CO and NO). *Phys. Chem. Chem. Phys.* **2006**, *8*, 407–417.
- (45) Kale, M. J.; Christopher, P. Utilizing Quantitative in Situ FTIR Spectroscopy To Identify Well-Coordinated Pt Atoms as the Active Site for CO Oxidation on Al2O3-Supported Pt Catalysts. *ACS Catal.* **2016**, *6*, 5599–5609.
- (46) Siemer, M.; Tomaschun, G.; Klüner, T.; Christopher, P.; Al-Shamery, K. Insights into Spectator-Directed Catalysis: CO Adsorption on Amine-Capped Platinum Nanoparticles on Oxide Supports. ACS Appl. Mater. Interfaces 2020, 12, 27765–27776.
- (47) Bazin, P.; Saur, O.; Marie, O.; Daturi, M.; Lavalley, J. C.; le Govic, A. M.; Harlé, V.; Blanchard, G. On the Reducibility of Sulfated Pt/CeXZr1-XO2 Solids: A Coupled Thermogravimetric FT-IR Study Using CO as the Reducing Agent. *Appl. Catal., B* **2012**, *119-120*, 207–216.
- (48) Fu, J.; Lym, J.; Zheng, W.; Alexopoulos, K.; Mironenko, A. V.; Li, N.; Boscoboinik, J. A.; Su, D.; Weber, R. T.; Vlachos, D. G. C–O Bond Activation Using Ultralow Loading of Noble Metal Catalysts on Moderately Reducible Oxides. *Nat. Catal.* **2020**, *3*, 446–453.
- (49) Prasomsri, T.; Shetty, M.; Murugappan, K.; Román-Leshkov, Y. Insights into the Catalytic Activity and Surface Modification of MoO3 during the Hydrodeoxygenation of Lignin-Derived Model Compounds into Aromatic Hydrocarbons under Low Hydrogen Pressures. *Energy Environ. Sci.* **2014**, *7*, 2660–2669.